RSC Advances

ROYAL SOCIETY OF CHEMISTRY

www.rsc.org/advances

Effect of solvent; enhancing the wettability and engineering the porous structure of calcium phosphate/agarose composite for drug delivery

Elayaraja Kolanthai[1,2], V. Sivaraj Dikeshwar Colon[3], P. Abinaya Sindu[3], V. Sarath Chandra[1], K.R.Karthikeyan[1], M. Surendar Babu[3], S. Meenakshi Sundaram[3], M. Palanichamy[4], S. Narayana Kalkura[1,*]

[1] *Crystal Growth Centre, Anna University, Chennai 600025, Tamil Nadu, India.*
[2] *Department of Materials Engineering, Indian Institute of Science, Bangalore-560012, Karnataka, India.*
[3] *Centre for Biotechnology, Anna University, Chennai 600 025, Tamil Nadu, India.*
[4] *Department of Chemistry, Anna University, Chennai 600025, Tamil Nadu, India.*

Abstract

Tissue engineering deals with the regeneration of tissues for bone repair, wound healing, drug delivery, etc., and highly porous 3D artificial scaffold is required to accommodate the cells and direct their growth. We prepared 3D porous calcium phosphate ((hydroxyapatite/β-tricalcium phosphate)/agarose, (HAp/β-TCP)/agarose)) composite scaffolds by sol-gel technique with water (WBS) and ethanol (EBS) as solvents. The crystalline phases of HAp and β-TCP in the scaffolds were confirmed by X-ray diffraction (XRD) analysis. The EBS had reduced crystallinity and crystallite size compared to WBS. WBS and EBS revealed interconnected pores of 1μm and 100 nm, respectively. Swelling ratio was higher for EBS in water and phosphate buffered saline (PBS). *In vitro* drug loading/release experiment was carried out on the scaffolds using gentamicin sulphate (GS) and amoxicillin (AMX). We observed initial burst release followed by sustained release from WBS and EBS. In addition, GS showed extended release than AMX from both the scaffolds. GS and AMX loaded scaffolds showed greater efficacy against *Pseudomonas* than *Bacillus* species. WBS exhibited enhanced mechanical properties, wettability, drug loading and haemocompatibility compared to EBS. In-vitro cell studies showed that over the scaffolds, MC3T3 cells has attached, proliferated and there was a significantly increase in live MC3T3 cells. Both scaffolds supported MC3T3 proliferation and mineralization

in the absence of osteogenic differentiation supplements in media which proves the scaffolds are osteoconducive. Microporous scaffolds (WBS) could assist the bone in-growth, whereas the presence of nanopores (EBS) could enhance the degradation process. Hence, WBS and EBS could be used as scaffold for tissue engineering and drug delivery. This is a cost effective technique to produce scaffolds of degradable 3D ceramic-polymer composites.

Keywords: Composites, Drug Delivery System, Wettability, Biocompatibility, Porous scaffold,

* E-mail: kalkura@gmail.com, kalkura@yahoo.com

Introduction

Highly bioactive and biocompatible scaffolds are synthesized for regeneration of large bone defects caused by bone diseases such as bone infections and bone cancer.[1] The current trend is to repair large bone defects by bone grafting materials such as autografts and allografts.[2] However, these have limitations due to limited availability and possibility of disease transmission.[2] Synthetic hydroxyapatite show poor bioactivity when implanted in the body. Hence, a bioactive material which mimics the natural cell environment is necessary for preparing functional scaffolds. Hydrogels/polymers are used for bone tissue engineering, as it mimics the physico-chemical properties of extracellular matrix with highly hydrated content having three dimensional structures.[3] Synthetic polymers such as poly(acrylic acid), poly(vinyl alcohol), polypeptides and natural polymers (collagen, agarose, chitosan) are used as scaffolds.[3] Such scaffolds have micropores to assist the drug delivery, cell attachment and fast tissue regeneration.[4] In addition, the surface wettability helps to grow cells, protein and drug loading on biomedical implants. However, polymer-based scaffolds display low mechanical properties. Hence, polymer/ceramic composites are fabricated to overcome this limitation.[5-7]

Agarose hydrogel is a biodegradable organic polymer matrix used for tissue engineering and drug delivery applications.[8] Agarose has gained acceptance in tissue engineering applications such as cell-hydrogel hybrids, nerve guidance scaffolds and micro patterned stamping arrays.[9] Tabata et al.[8] reported that HAp/agarose composites showed high osteoconductivity as well as biodegradability. Freeze dried β-TCP/agarose and poly(ethylene glycol) with β-TCP/agarose scaffolds behave like a reinforced hydrogel.[10] HAp/agarose and calcium carbonate/agarose composite gels synthesized by Swzawa et al.[11] activated new bone formation. HAp/agarose composites induced osteoconduction and increased the recovery periods compared to pure agarose hydrogel.[12]

Microorganisms such as *S. aureus*, *S. epidermidis* cause infection and osteomyelitis of the bone or bone marrow on implantation. The antibiotic delivery systems for the treatment/ bone infection are important because of the poor blood circulation in the osseous tissue which needs the supply of large amount of antibiotics to reach the adequate therapeutic level in the affected region.[13] Hence, the controlled release of drug from the bone implant scaffold is essential to prevent the osteomyelitis disease. Antibiotic loaded bone implant is used for the treatment of osteomyelitis for preventing osseous staphylococcal infections by local drug delivery.[14] The porous scaffold is fabricated by various methods such as solvent casting, emulsion free and freeze drying, etc. Freeze drying method helps to preserve the structure intact without shrinkage and tailors the porosity. Here, we report the preparation of (HAp/β-TCP)/agarose scaffold using aqueous and organic solvents by sol-gel technique. Antibiotics loading/release and *in vitro* biological performance of the scaffolds were also investigated.

Experimental

Materials

Analytical grade calcium nitrate tetrahydrate ($Ca(NO_3)_2.4H_2O$, Merck), diammonium hydrogen phosphate ($(NH_4)_2HPO_4$, Merck), agarose gel ($C_{10}H_{15}N_3O_3$, SRL), ammonia solution (Merck), ethanol (Merck) and deionized water were used for scaffold preparation. $(NH_4)_2HPO_4$ (0.3 M) was dissolved in 250 mL of deionized water under continuous stirring at 85°C. Agarose (3 W/V %) was added into the phosphate solution for gelation. $Ca(NO_3)_2.4H_2O$ (0.5 M) was dissolved in 250 mL of deionized water and it was added into phosphate with agarose solution at constant flow rate for 3 h. During the reaction, pH of the solution was maintained at 10.5 using ammonia solution. After mixing, the sol was stirred continuously for 3 h with pH 10.5. The sol-gel was washed using deionized water and was poured into Petri dish and allowed to gel at room temperature. After gelation, the samples were frozen at -20 ˚C and freeze dried at -54 °C for 8 h. Similarly, ethanol based scaffolds were prepared by replacing water with ethanol. Ammonia solution was used to maintain a constant pH of 10.5. The water and ethanol based scaffolds were named WBS and EBS respectively and photographic image of freeze-dried WBS and EBS are as shown in figure 1.

Characterization

The crystalline phase of the scaffolds were analyzed by X-ray diffraction analysis using PANalytical X'pert Pro diffractometer, CuKα radiation (λ = 1.5406 Å) with 40 kV and 30 mA. The XRD was recorded in the range from 10 to 70° with increment step of 0.02°/s. All the crystalline planes were indexed and their full width half maximum was analyzed by XRDA software. The crystallite size (L) was determined using Scherrer formula from the XRD data.[15] The degree of crystallinity was determined by empirical relation $\beta_{002} \times (X_c)^{1/3} = K_A$, where X_c is the degree of crystallinity, β_{002} the full width of the peak at half intensity of (002) reflection in degree, K_A is a constant set at 0.24.[15] The functional groups of the scaffolds were determined by Fourier transform infrared (FTIR) spectroscopy. The powdered scaffold was mixed with KBr

and pressed into pellets. The spectrum was recorded by transmission mode in the range of 400 to 4000 cm^{-1} using Perkin-Elmer spectrum RXI FTIR system with resolution of 2 cm^{-1}. The surface morphology of the gold coated samples was examined using scanning electron microscope (SEM, Hitachi S-3400N) at 15 kV. The wettability (30 °C) of the scaffold surface was investigated by water contact angle measurement as described in our previous report.[16] The thermogravimetric (TGA) and differential thermal analyses (DTA) of the samples were carried out between 30 and 900 °C under nitrogen atmosphere at a heating rate of 20 °C/min. Haemolysis test was performed on the WBS and EBS scaffolds. Fresh human blood was collected in a sterile centrifuge tube which contains heparin to avoid the clot formation. 100 mg of both scaffolds were equilibrated by 1 mL of sterile saline and it's incubated at 37 ºC for 12 h. After incubation, the saline was removed and 250 µL of human blood was added into the scaffolds and kept at 37 ºC for 20 min. Finally, 4 mL of saline (0.9 % W/V NaCl) was added to each scaffold to stop the haemolysis. Positive and negative controls were prepared by adding 250 µL of human blood in 5 mL of water and saline. Incubated scaffolds were centrifuged at 1000 rpm for 5 min. The optical density of the supernatant solution was measured at 545 nm using UV-visible spectrometer (UV-1601 Shimadzu). The percentage of haemolysis was calculated as per the formula given below and their values were plotted in graph. (%) of Haemolysis = {[OD (scaffold) − OD (negative control)]/[OD (positive control) − OD (negative control)]} × 100. The accepted norm of haemolysis percentage is (i) Highly haemocompatible (< 5% haemolysis), (ii) Haemocompatible (within 10 % haemolysis) and (iii) Non-haemocompatible (> 20 % haemolysis).[17] The *in vitro* bioactivity of the scaffolds was investigated using simulated body fluid (SBF).[18, 19] The samples (100 mg) were immersed into 20 mL SBF solution and incubated at 37 °C for a period of one to four weeks. The *in vitro* swelling behavior of WBS and EBS were studied by exposing into 20 mL of deionized water,

phosphate buffer saline (PBS, pH 7.4) and simulated body fluid (SBF) at 37 °C. Swelling of the scaffolds was monitored gravimetrically before and after immersion in solutions by measuring weight with respect to time for 24 h. The experiment was carried out in triplicate and the wet weight of the scaffolds was determined by removing the sample from the swelling media and wipes the surface water of the scaffold using Whattmann filter paper. The swelling ratio $E_{(sr)}$ in percentage, which corresponds to the average hydration degree has been determined according to the following equation.[10]

$$E_{(sr)}\ (\%) = ((W_s - W_d)/ W_d)\times 100$$

where, $E_{(sr)}$ is the amount of water absorbed (weight percent) by the scaffolds and W_s, W_d are the weights of the scaffolds in swollen and dried state respectively.

Mechanical Testing

Compression testing of the scaffolds was carried out using Mechanism micro universal testing machine (UTM) with 500 N load cell and data acquisition software. Circular disc of (10 mm dia with ~3 mm thick) WBS and EBS scaffolds were used for mechanical analysis. The samples were placed between two parallel palates and loaded at a rate of 1mm/min which is approximately strain rate of 2 % (0.016 s^{-1}). All the scaffolds were tested at pre-load of 0.03 N and each specimen was subjected to 60 % strain. The compressive modulus was calculated from the slope at strain value of 10 %, 25 % and 50 % of the resulting stress-strain curve.

Biocompatibility test

MC3T3-E1 subclone 4 mouse osteoblast cell lines (ATCC)) were cultured in eagles minimum essential medium (α-MEM, Invitrogen), supplemented with 10% Fetal Bovine Serum (FBS, Invitrogen), 10 μg/mL streptomycin (Invitrogen), 10 μg/mL penicillin and culture was incubated at 37 °C in a humidified atmosphere with 5 % CO_2. The medium was changed every two days until 80% to 90% confluency then sub-culture the cells. The cells monolayer was

washed twice with PBS solution and detached from their culture flask by incubating with 0.25 % Trypsin-EDTA (Gibco) solution for 3 min. Detached MC3T3 cells of 1 x 10^4 (Passage 16) were seeded in each well of 48 well tissue culture plates containing three time washed with PBS samples of WBS and EBS (size 10 mm of disc and ~3 mm thick) to remove the un-reacted products.

The cell proliferation was studied using MTT assay on 1, 3 and 7 days. At each time point, 400µL of MTT reagent (1mg/mL) was added to each well and incubated for 4 h at the same condition. Finally, MTT reagent was removed and 400µL of dimethyl sulfoxide (DMSO) (Sigma-Aldrich) was added for dissolving the formasan crystals and the absorbance was measured at 570 nm in an ELISA (Thermo Scientific) reader. For statistical analyses, 1-way ANOVA (analysis of variance) with Tukey's test for multiple comparisons was used and differences were considered statistically significant if $p < 0.05$.

After each culture time point, cells on the samples were stained using live/dead assay kit (Molecular Probes), containing calcein AM and ethidium homodimer. Non-fluorescent cell-permeant calcein AM will be enzymatically converted to intense green fluorescent calcein in live cells, while ethidium homodimer enters cells with damaged membranes, binding to nucleic acids and producing a bright red fluorescence in the dead cells. At each time point, the media was discarded and the samples were washed with PBS, then live/dead solution containing 2 mM calcein AM and 4 mM ethidium homodimer was added to each well and were incubated at 37 ºC for about 20 min. The stained cultures were viewed using fluorescent microscope.

The attachment and spreading of MC3T3 cells on the scaffolds were examined using Alexa Fluor 546 Phalloidin/DAPI staining. After 1, 3 and 7 days of incubation, cell seeded composite scaffolds were fixed with 3.7% formaldehyde for 30 min and rinsed with water. After

cell fixing, 0.2 % Triton X-100 in water was added on scaffolds for permeabilization and incubated for 15 min. Then the scaffolds were washed with water and stained with 200 µl of Alexa Fluor 546 Phalloidin for 45 min and 200 µl of DAPI dyes commonly used for F-actin and nuclei imaging respectively for 10 min in the dark environment. The scaffolds were then washed with deionized water and viewed under fluorescent microscope (Olympus-BX-51) after removing the excess water.

In vitro mineralization was studied before and after cell cultured on WBS and EBS scaffolds for 7 and 14 days using Alizarin red S assay. After each time point, cells were fixed with 3.7 % formaldehyde for 30 min and stained with 2 % Alizarin red S dye (AR) for 20 min and washed several times with deionized water to remove excess stain. Digital images of stained scaffolds were recorded. To retain the bound stain from scaffolds, samples were treated with 0.5 mL of 0.5 N HCL containing 5% SDS for 30 min. The absorbance of the dissolved AR stain was measured at 415 nm in an ELISA (Thermo Scientific) reader and quantified.

Drug loading/Release

250 mg of gentamicin sulphate (GS) and 150 mg of amoxicillin (AMX) drugs were dissolved separately in 10 mL of deionized water. 500 mg of WBS and EBS scaffolds were soaked in drug solutions. These solutions were kept at room temperature for 24 h in incubator cum orbital shaker with a shaking speed of 100 rpm. Subsequently, the supernatant solution was removed and the absorbance was measured at λ = 248 and 230 nm using UV-Vis spectrophotometer (Shimadzu UV-1601). Percentage of drug loading was calculated using the formula, Percentage of drug loading = $[(Y-X)/X] \times 100$, where, X represents the initial concentration of the drug and Y, the final concentration of drug after removing the scaffold from the drug solution. The drug (GS, AMX) loaded scaffolds were dried at 37 °C and named as

WBS-GS, EBS-GS, WBS-AMX and EBS-AMX. The drug release study was carried out using PBS (pH-7.4). The drug loaded scaffolds in triplicates was kept in 100 mL of dissolution medium (PBS) and was incubated at 37 °C with shaking speed of 100 rpm. At different time interval, 1 mL of drug solution was removed and replenished with the equal amount of PBS. The drug release was followed by absorption measurement at wavelength, λ = 248 and 230 nm which is the respective maximum absorbance of GS and AMX drugs using UV-Vis spectrophotometer. [13, 16]

Antimicrobial activity

The bacterial resistance of the scaffolds was investigated using *Pseudomonas aeruginosa* and *Bacillus* species. 300 μL of the culture ($1x10^5$ Colony Forming Units/mL) was uniformly spread on Muller-Hinton agar plates. After spreading, same size of as prepared and drug (GS and AMX) loaded scaffolds were placed on MH agar plate. The plates were incubated at 37 °C for 24 h and inhibition zone was noticed every 3 h.[16]

Results and discussion

XRD analysis

The XRD patterns of WBS and EBS are shown in figure. 2(a). The peaks were corresponding to that of HAp (JCPDS no: 09-0432) and β-TCP (JCPDS data no: 09-0169). Low intensity planes (111), (210), (300) and (221) were well resolved than major (211) plane of HAp. This might be due to the preferential growth of HAp in agarose gel matrix along the (111), (210), (300) and (221) planes.[19] In addition, the crystallographic planes shift by 0.3° towards lower 2θ, indicating a reduction in lattice parameters due to presence of agarose. This reveals the interaction between agarose with HAp and β-TCP particles.[20] In addition, the reduction in intensity of (211) plane, could be attributed to the presence of agarose and β-TCP in the composite.[21] The lattice parameters, unit cell volume, degree of crystallinity and average

crystallite size were calculated and are shown in Table 1. The average crystallite size was found respectively to be 80 and 60 nm for WBS and EBS. The degree of crystallinity of EBS was found to be nearly half of that of WBS (Table 1). The alcohol based synthesis seemed to reduce the crystallite size and degree of crystallinity (50%) compared to water based synthesis. The crystallization was rapid in ethanol and so crystallinity was lower than that of water. The purpose of agarose is to regulate the growth of TCP and to act as a binder. It forms a three dimensional viscous matrix by which the supply of ingredients of TCP is regulated during growth.

FTIR

The FTIR spectrum of scaffolds is shown in figure 2(b). The broad band between 3600-2600 cm^{-1} was due to OH stretch of water, agarose and NH stretch of NH_4^+ in WBS and EBS.[22] The peak at 1637 cm^{-1} and 1384 cm^{-1} is due to bending vibration of water and CH_2 of agarose. The CH_2 stretching vibration of agarose below 3000 cm^{-1} was not well resolved. The P-O vibration of phosphate group occurs at 1032 cm^{-1}. In pure HAp, this peak appears as a triplet with peaks well resolved at 1096, 1085 and 1056 cm^{-1}. The presence of agarose and TCP phase in WBS and EBS scaffold leads to peak broadening.[23] The peak due to the non-degenerate P-O symmetric stretching mode appeared as a weak peak at 961 cm^{-1}. The peaks at 932 cm^{-1} and 890 cm^{-1} were attributed to the C-O-C stretching of agarose.[24] The bands at 602 cm^{-1} and 563 cm^{-1} correspond to the triply degenerate O-P-O bending mode and the low intensity peak at 632 cm^{-1} was due to the OH stretching vibration.[22] The hydroxyl band shows reduced peak area in WBS scaffold due to presence of TCP phase, indicating the biphasic nature of WBS and EBS.[20] When compared with WBS and EBS, broad band was observed between 3600 and 2500 cm^{-1} for WBS-GS and EBS-GS. The N-H vibration and C-H vibration between 3600 and 2500 cm^{-1} was not clearly resolved. All other peaks in the fingerprint region were similar to WBS, but for the

appearance of a sharp peak at 1118 cm^{-1}, assigned to C-O vibration of GS. The weak peak at 602 cm^{-1} is owing to the phosphate bending mode. The intensity of the peak at 3151 cm^{-1} of EBS was low, whereas increase in intensity was observed at 3440 cm^{-1} and 1122 cm^{-1} for EBS-GS. The variation of intensities and appearance of new peaks in WBS-GS and EBS-GS compared with WBS and EBS could be due to the loading of GS. Similar features were observed for AMX loaded scaffolds (spectra not shown).

TGA/DTA

TGA/DTA thermogram of WBS and EBS are shown in figure 2(c). TGA showed four distinct stages of weight loss for WBS. The initial weight loss (11 %) observed at less than 100 °C corresponds to the loss of absorbed surface water. The major weight loss (34 %) between 150 and 210 °C is attributed to the decomposition of agarose and nitrates. Third weight loss (17 %) between 250 and 350 °C is due to the decomposition of agarose. The fourth weight loss (13 %) between 350 and 600 °C is owing to the condensation of hydroxyl group of HAp and removal of organic additives. The EBS showed three different stages of weight loss. Initial weight loss (16 %) below 100 °C corresponds to the desorption of surface ethanol. Second weight loss (36 %) between 150 to 210 °C is due to the decomposition of agarose and nitrates. Third weight loss (11 %) between 250 to 550 °C is due to the decomposition of agarose, condensation of hydroxyl group of HAp and removal of organic additives. There is no weight loss above 600 °C in both scaffolds. The residue of WBS and EBS were 25 % and 37 %, respectively. The EBS exhibited better thermal stability than WBS due to the presence of nanosized particles of HAp.[25]

SEM

SEM micrograph of WBS and EBS are in figure 3(a-d). The WBS surface showed uniform spherical particles of 3 to 4 μm (Figure 3a) having interconnected pores (1-2 μm)

(Figure 3b), whereas, EBS was spongy consisting of spherulites (0.5 μm) with interconnected nano pores (100-200 nm) (Figure 3c-d). The solvent, ethanol plays an important role in the reduction of particle and pore size in EBS when compared to WBS. The electrostatic force between the ions in ethanol is higher than water, which enhanced the formation of HAp crystals as predicted by Coulomb's law. The electrostatic forces are inversely proportional to the dielectric constant (relative permittivity) of the solvent. The dielectric constant is higher in water (78) than in ethanol (24). Stronger and longer range interactions between the ions in organic solvents could be expected to achieve faster reaction and nucleation rates leading to the formation of smaller particles with regular morphology.[26] Osteoconductivity of the bone implants depends on the type of scaffold used and its porosity. Tabata et al reported that HAp/agarose composites without pores were osteoconductive and could be used as an alternative biodegradable bone-graft material in humans.[8] Here, the presence of micropores (<50 μm) would allow blood capillaries to grow inside and facilitate the nutrient transportation in the scaffold for the tissue engineering and drug delivery applications.[27] The large surface area provided by the nanopores regulate the degradation process of the scaffolds and in addition enhances cell response.[28]

Wettability

The wettability of a flat surface is expressed by the contact angle θ between a liquid drop and a solid surface due to intermolecular interactions described by Young's equation.[16] The contact angle of water was measured on the surface of WBS and EBS (Figure 3(e-f)). The contact angle between WBS and water drop was 5±1 ° (Figure 2e) and EBS was 42±1° (Figure 2f) at 1 S. The results suggested that WBS was more hydrophilic than EBS scaffold. When implanted in human body, hydrophilic material will facilitate homogeneous and sufficient cell

attachment throughout the porous scaffold. In addition, the protein adsorption, antibiotic loading and proliferation will increase on hydrophilic surface of the scaffolds.[29]

In vitro bioactivity study

A dense spherulitic apatite deposition (0.5 to 2 μm) was observed on the WBS surface after two weeks of immersion in SBF (Figure 3g). In the case of EBS, uniform layer of apatite was deposited on the surface (Figure 3h). WBS displayed better *in vitro* bioactivity than EBS. The pH (7.4 to ~ 7.1) of the SBF was found to initially decrease on immersion of the samples in a week, due to the partial dissolution of the agarose (weak adsorption on the external surface) from the scaffolds.[19] Subsequently, the pH of the SBF increased to ~ 7.6 by the end of the fourth week, indicating the apatite layer deposition on the scaffolds.[19] The apatite formation was further confirmed, by studying the difference between weights of the scaffolds before and after immersion. An initial weight loss of about 30 and 50 % was observed respectively for WBS and EBS during the first week of immersion. Subsequently, the weight of WBS and EBS were found to be increased by 28 and 20 %, respectively. The initial weight loss was due to the fast degradation rate of agarose in SBF than the deposition of apatite particles. After a week, apatite deposition was dominating over degradation as indicated by the increase in weight of the scaffolds.

Mechanical Testing

The stress-strain curve by compressive test carried out on freeze-dried WBS and EBS scaffold shown in figure 4. The compressive modulus and strength of the scaffolds showed gradual increment with increase in strain rate. Compressive modulus at 50 % strain was 60.88±1.54 MPa and 48.95±4.98 MPa in WBS and EBS respectively (Table 2). The slight variation in the compressive modulus may be due to the differences in the porosity of the scaffolds. The initial compressive modulus was low for the both the scaffolds because agarose

gel gets dense with hydroxyapatite nanoparticles, subsequently nanoparticles resist the compressive force, giving rise to a higher modulus value.

Haemolysis

The haemolysis percentage of WBS and EBS was found to be 6 and 10 % respectively, which were well within the acceptable limits of a biocompatible material.[17] The variation in haemocompatibility in EBS scaffold when compared with WBS may be attributed to the inclusion of the solvent. The WBS scaffold could be preferred as wound dressing material or implantable drug delivery system owing to their better haemocompatibility.[17]

In vitro swelling behavior

The percentage of swelling ratio ($E_{(sr)}$) versus time of immersion of both the scaffolds in different solutions is shown in figure 5a. We observed initial rapid increase in $E_{(sr)}$ upto 4h on immersion in water, PBS and SBF solutions, followed by a slow rate of increment in $E_{(sr)}$ upto 20 h, before reaching equilibrium. Equilibrium $E_{(sr)}$ was found to be respectively between 10 and 60 % for WBS and EBS. When compared with immersion in PBS (42 %) and SBF (28 %) solutions, swelling ratio significantly increased in water (60 %) for EBS. EBS showed higher $E_{(sr)}$ than WBS in PBS and water, due to the presence of large number of nanosized pores and particles. In addition, agarose behaves like a hydrogel and is responsible for the enhanced absorption of water and PBS. The physical properties of agarose are similar to those of living tissues which assist in fast healing of wound area.[8] During swelling process, the volume of the scaffolds increased without any significant change in shape. The photographic image of native and 24 h PBS soaked swollen WBS and EBS is shown in figure 5b and 5c. This property will help to ensure a good fit between the sample and osseous defect. The scaffolds could adsorb physiological fluids and yield controllable augmentation on implantation, having a beneficial effect on osteoblast growth and differentiation. Further, this

study may provide an insight into the degradation mechanism of the scaffolds during implantation in living organisms.[10]

Drug loading and release

GS and AMX can be loaded into porous WBS and EBS scaffold by impregnation process by immersing them in drug solution. The OH groups on the WBS and EBS surface react with NH_2 group in GS and carboxyl group in AMX to form hydrogen bonding, leading to higher encapsulation of the drugs.[21] The weight percentage loading of the AMX was 45±1, 40±1 and GS was 70±1, 54±1 on WBS and EBS respectively. WBS exhibited enhanced loading of AMX and GS. The drug encapsulation depends on the porosity, size, shape, distribution, connectivity, potential functionalization of their walls and wettability of the surface.[30] In addition; size, nature and dimensions of the drug to be introduced also play a role. Here, the respective molecular size of GS and AMX were 0.9 nm and 1.1 nm. SEM images revealed macro porous WBS surface (1-2 μm), whereas EBS consisted of nanosized pores (100-200 nm) (Figure 2b and 2d). In addition, WBS was more hydrophilic than EBS. Therefore, large size of pores and hydrophilic nature of surface, play a major role in enhancing the encapsulation of drug in WBS.[31] The drug loading capacity of EBS was low due to the small pore size and low hydrophilic surface compared with WBS.[30]

Hydrogel scaffolds are preferred as biomedical implants and drug delivery systems. The drug loaded samples were subjected to drug release in PBS. During the drug release process, PBS enters into the drug loaded samples through the pores. The drug is then slowly released into PBS from the surface and through the pores. The cumulative drug release profiles as a function of release time in PBS is shown in figure. 6. We observed 80 and 76 % drug release respectively from WBS-AMX and EBS-AMX in 1 h. The drug release from WBS-GS and EBS-GS was respectively 68 and 66 %. Both the drug release profiles showed initial burst release which may

be attributed to the physisorption of GS and AMX on the outer surface of the scaffolds and the high degradation rate and rapid swelling of the hydrogel in WBS and EBS. In addition, the burst release of water soluble drugs from dehydrated agarose with HAp matrix generally involves the simultaneous absorption of water, and desorption of drug via a swelling-controlled diffusion mechanism.[31] The drug release in hydrophilic samples occurs at a rate relative to sample swelling and influenced by factors such as presence of pores and the entrapment of drugs. The burst release is observed during first 1 h, which agree with the fast uptake of OH groups from PBS and it initiates the faster drug release. Burst release will provide efficacy against micro-organisms after surgery. AMX drug showed controlled release of 95 and 96 % from WBS-AMX and EBS-AMX respectively at 6 h. However, 97 and 93 % GS drug was released from WBS-GS and EBS-GS respectively in 27 h. These results suggested that water soluble drugs are released faster due to the porous and hydrophilic nature of the scaffolds.[31] Hydrophilic drugs delivered through hydrogel systems typically have a release period of hours to days. In the case of the local drug delivery system, initial burst release leads to the immediate killing of the microorganism at the drastically damaged tissues and sterilizes of the infected site. Since bone have the poor blood supply, the gentamicin concentrations will probably be higher in bone than in the buffer media and consequently sustain for a longer time above the MIC at in vivo conditions. Lambotte et al reported that gentamicin released from the scaffold within three days in bone, however, the antibiotic effect still remained upto 10 days.[32] Therefore, GS and AMX loaded WBS and EBS may provide the MIC concentrations of gentamicin and sustain longer in bone.

Antimicrobial Activity

Antimicrobial activity of the samples was analyzed using *Pseudomonas* and *Bacillus* species. There was no bacterial resistant zone observed in drug free WBS and EBS. The WBS-GS, EBS-GS, WBS-AMX and EBS-AMX had shown gradual increase in inhibition zone for

Pseudomonas and *Bacillus* (Table 3). *Pseudomonas* had greater inhibition zone than Bacillus for WBS-GS, EBS-GS, WBS-AMX and EBS-AMX. WBS-AMX and EBS-AMX showed the smallest inhibition zone compared to WBS-GS and EBS-GS. This suggested that release of GS was higher than AMX from both the scaffolds. Diameter of inhibition zone for all the samples were gradually increased, due to the controlled release of drug.

Biocompatibility study

The proliferation of MC3T3 cells cultured on WBS and EBS scaffolds for 1, 3 and 7 days was compared using MTT assay (Figure 7). The proliferation of MC3T3 cells was higher in WBS then EBS at every time point. The results indicate that WBS is more suitable for osteoblast cell growth than EBS. Figure 8 (a-f) shows MC3T3 cells stained with live/dead reagent (Live cells are stained green, dead cells red). The number of live cells increased with increase in culture time and few dead cells on both scaffolds were indicated by arrow. These results corroborated with cell proliferation assay (MTT assay) results.

Fluorescent images of Alexa Fluor 546 Phalloidin/DAPI staining of cells incubated for 1, 3 and 7 days on the WBS and EBS were shown in figure 9 (a-f). The cells were attached and distributed throughout the scaffold. An enhanced cell proliferation was seen on WBS compared to EBS due to the highly hydrophilic nature. The cells attached, spread and proliferated throughout out the culture period on both the samples due to the presence of nHAp, which aids the adsorption of proteins on the scaffold surfaces. These adsorbed proteins attract more number of cells, enhancing the cell attachment and proliferation.

In vitro mineralization of MC3T3 on 3D scaffolds without osteogenic supplement in media for 7 and 14 day observed using Alizarin Red S assay. Photographic image clearly showed that the deposition of calcium mineral on WBS scaffold increased with increase in culturing time (Figure 10a). Bound alizarin dye optical density (OD) of cell cultured samples

was subtracted from OD value of samples without cells. Figure 10 b shows the calcium mineral deposition during MC3T3 cell growth. These results showed increase in absorbance value from day 7 to day 14 which indicates that the calcium mineral deposition increased with increasing culturing time. WBS has shown the high calcium deposition than EBS.

Conclusion

Tissue engineering is a promising approach for the treatment of defective and lost bone. The biodegradable and osteoconductive scaffolds with a 3D interconnected porous network would be useful for the fabrication of biomedical implants. The present study show the feasibility of producing cost effective freeze dried organic-inorganic composite scaffolds for tissue engineering and drug delivery applications. Biphasic calcium phosphate made up of resorbable β-TCP and non-resorbable HAp phases in WBS and EBS were produced and both scaffolds showed 60 % of HAp/β-TCP and 40 % of agarose in composites. The thermal stability and swelling ratio of EBS were higher than WBS. The ethanol and water based synthesis respectively yield nano and micropores scaffolds having interconnected pores. From these studies, we conclude that the pore size of the scaffold can be engineered by varying the solvent. We observed enhanced encapsulation of drugs, GS and AMX, in WBS due to large size of pores and enhanced surface wettability. Burst release followed by the controlled drug release was exhibited by both types of scaffolds. *Pseudomonas* was more resistant in GS and AMX than *Bacillus* species. WBS showed enhanced wettability, interconnected pores, bioactivity, haemocompatibility, drug loading and mechanical properties than EBS. Cell studies proved that WBS was most effective in promoting MC3T3 mouse osteoblast cell attachment, proliferation and osteoconductivity. WBS and EBS seem to be respectively suitable for tissue engineering and drug delivery application. This fabrication technique which is cost effective and fast, yield 3D scaffolds with uniformly distributed bioceramics in a degradable polymer matrix.

Acknowledgements

One of the authors (K.E) acknowledges CSIR, India for the award of SRF fellowship (File No. 09/468(0413)2009-EMR-I). This work was supported by the Department of Biotechnology, New Delhi through a research project (No.BT/PR11799/MED/32/2009).

References

[1] M. Braddock, P. Houston, C. Campbell and P. Ashcroft, Born Again Bone: Tissue Engineering for Bone Repair, *News Physiol. Sci.* 2001, **16**, 208-13.

[2] G. Wei and P.X. Ma, Structure and properties of nano-hydroxyapatite/polymer composite scaffolds for bone tissue engineering, *Biomaterials* 2004, **25**, 4749-57.

[3] K.Y. Lee and D. J. Mooney, Hydrogels for Tissue Engineering, *Chem. Rev.* 2001,**101**,1869-79

[4] E. Sachlos, N. Reis, C. Ainsley and J. T. Czernuszka, Novel collagen scaffolds with predefined internal morphology made by solid free form fabrication, *Biomaterials* 2003, **24**, 1487-97

[5] K. Rezwana, Q. Z. Chena, J. J. Blakera and A.R. Boccaccinia, Biodegradable and bioactive porous polymer/inorganic composite scaffolds for bone tissue engineering, *Biomaterials* 2006, **27**, 3413-31.

[6] M. I. Sabir, X. Xu and L. Li, A review on biodegradable polymeric materials for bone tissue engineering applications *J. Mater. Sci.* 2009, **44**, 5713-24.

[7] I. Armentano, M. Dottori, E. Fortunati, S. Mattioli and J. M. Kenny, Biodegradable polymer matrix nanocomposites for tissue engineering: A review, *Polymer Degradation and Stability* 2010, **95**, 2126-46.

[8] M. Tabata, T. Shimoda, K. Sugihara, D. Ogomi, T. Serizawa and M. Akashi, Osteoconductive and Hemostatic Properties of Apatite Formed on/in Agarose Gel as a Bone-Grafting Material, *J. Biomed. Mater. Res. B Appl. Biomater.* 2003, **67**, 680-8.

[9] Y. Lin, S. Tang, X. Mao and L. Bao, Protein recognition via molecularly imprinted agarose gel membrane *J. Biomed. Mater. Res. A* 2008, **85**, 573-81.

[10] J. Roman, M. V. Cabanas, J. Pena, J.C. Doadrio and M. Vallet-Regi, An optimized β-tricalcium phosphate and agarose scaffold fabrication technique, *J. Biomed. Mater. Res. A* 2008, **84**, 99-107.

[11] Y. Suzawa, T. Funaki, J. Watanabe, S. Iwai, Y. Yura, T. Nakano, Y. Umakoshi and M. Akashi, Regenerative behavior of biomineral/agarose composite gels as bone grafting materials in rat cranial defects, *J. Biomed. Mater. Res. Part A* 2010, **93,** 965-75.

[12] J. Watanabe, M. Kashii, M. Hirao, K. Oka, K. Sugamoto, H. Yoshikawa and M. Akashi, Quick-forming hydroxyapatite/agarose gel composites induce bone regeneration, *J. Biomed. Mater. Res. Part A* 2007, **83,** 845-52.

[13] V. Mourino and A. R. Boccaccini, Bone tissue engineering therapeutics: controlled drug delivery in three-dimensional scaffolds, *J. R. Soc. Interface* 2010, **7**, 209-27.

[14] M. E. Husseiny, S. Patel, R. J. MacFarlane, F. S. Haddad, Biodegradable antibiotic delivery systems *J. Bone Joint Surg.* 2011, **93**, 151-7.

[15] V. M. Rusu, C. H. Ng, M. Wilke, B. Tiersch, P. Fratzl and M. G. Peter, Size-controlled hydroxyapatite nanoparticles as self-organized organic–inorganic composite materials, *Biomaterials* 2005, **26**, 5414-26.

[16] K. Elayaraja, P. Rajesh, M.I. Ahymah Joshy, V. Sarath Chandara, R.V. Suganthi, J. Kennedy, P. K. Kulriya, I. Sulania, K. Asokan, D. Kanjilal, D. K. Avasthi, H. K. Varma and S. N. Kalkura, Enhancement of wettability and antibiotic loading/release of

hydroxyapatite thin film modified by 100 MeV Ag^{7+} ion irradiation, *Mater. Chem. Phys.* 2012, **134**, 464-77.

[17] V. Sarath Chandra, B. Ganga, R. V. Suganthi, K. Elayaraja, M. I. Ahymah Joshy, W. S. Beaula, R. Mythili, V. Ganesh, K. Sivakumar and S. Narayana Kalkura, Blood Compatibility of Iron-Doped Nanosize Hydroxyapatite and Its Drug Release *Appl.Mater.Interface* 2012, **4**, 1200-10

[18] T. Kokubo and H. Takadama, How useful is SBF in predicting in vivo bone bioactivity? *Biomaterials* 2006, **27**, 2907-15.

[19] M. I. Ahymah Joshy, K. Elayaraja, R.V. Suganthi and S. Narayana Kalkura, Mineralization of oriented nano hydroxyapatite in photopolymerized polyacrylamide gel matrix, *Cryst. Res.Technol.* 2010, **45,** 551-6.

[20] V. Siva Kumar and K. P. Rao, Preparation, characterization and in vitro release of gentamicin from coralline HAp-gelatin composite microspheres, *Biomaterials* 2002, **23**, 3175-81.

[21] P. Kumar, K. H. Prakash, P. Cheang, L. Gower and K. A. Khor, Chitosan-mediated crystallization and assembly of hydroxyapatite nanoparticles into hybrid nanostructured films, *J. R. Soc. Interface* 2008, **5**, 427-39.

[22] T. K. Anee, M. Ashok, M. Palanichamy and S. Narayana Kalkura, A novel technique to synthesize hydroxyapatite at low temperature, *Mater. Chem. Phys.* 2003, **80**, 725-30.

[23] I. Manjubala and M. Sivakumar, In-situ synthesis of biphasic calcium phosphate ceramics using microwave irradiation, *Mater. Chem. Phys.* 2001, **71**, 271-8.

[24] V. Sanchez-Vaquero, C. Satriano, N. Tejera-Sanchez, L. Gonzalez Mendez, J. P. Garcia Ruiz and M. Manso Silvan, Characterization and cytocompatibility of hybrid aminosilane-agarose hydrogel scaffolds *Biointer. phases* 2010, **5**, 23-29.

[25]. R. Murugan and S. Ramakrishna, "Bioresorbable composite bone paste using polysaccharide based nano hydroxyapatite", Biomaterials 2004, 25, 3829-35.

[26] H. Alobeedallah, J. L. Ellis, R. Rohanizadeh, H. Coster and F. Dehghani, Preparation of Nanostructured Hydroxyapatite in Organic Solvents for Clinical Applications, *Trends Biomater Artif Organs* 2011, **25**, 12-19.

[27] P. Fabbri, V. Cannillo, A. Sola, A. Dorigato and F. Chiellini, Highly porous polycaprolactone-45S5 Bioglass scaffolds for bone tissue engineering *Compos. Sci. Technol.* 2010, **70**, 1869-78.

[28] S. Wang, M. M. Falk, A. Rashed, M. M. Saad, A. C. Marques, R. M. Almeida, M. K. Marei and H. Jain, Evaluation of 3D nano–macro porous bioactive glass scaffold for hard tissue engineering *J. Mater. Sci: Mater. Med.* 2011, **22**, 1195-203.

[29] L. Safinia, K. Wilson and A. Bismark, Atmospheric Plasma Treatment of Porous Polymer Constructs for Tissue Engineering Applications, *Macromol. Biosci.* 2007, **7**, 315-27.

[30] M. Vallet-Regi, Ordered Mesoporous Materials in the Context of Drug Delivery Systems and Bone Tissue Engineering *Eur J* 2006, **12**, 5934-43.

[31] Z. N. Al-Sokanee, A. A. H. Toabi, M. J. Al-assadi and E. A. Alassadi, The Drug Release Study of Ceftriaxone from Porous Hydroxyapatite Scaffolds *AAPS PharmSciTech* 2009, **10**, 772-9.

[32] J.C. Lambotte, H. Thomazeau, G. Cathelineau, G. Lancien, J. Minet and F. Langlais, Tricalcium phosphate, an antibiotic carrier: A study focused on experimental osteomyelitis in rabbits, *Chirurgie* 1998, **123,** 572–579.

[33] Y. Xia, P. Zhou, X. Cheng, Y. Xie, C. Liang, C. Li and S. Xu, Selective laser sintering fabrication of nano-hydroxyapatite/poly-ε-caprolactone scaffolds for bone tissue engineering applications, *Inter. J. Nanomedicine* 2013, **8,** 4197–4213.

List of Tables

List of the figures

fluorescence microscope images of WBS (a, c, e) and EBS (b, d, f). (Blue indicates nucleus and Red indicates cell cytoplasm). The insert represent higher magnification of cell image of WBS and EBS. Scale bar represents 80 μm.

Figure 10 (a) Photographs of calcium mineral deposition on WBS and EBS measured using Alizarin Red S assay and (b) absorbance plot for retained dye from mineralized sample at 415 nm for 7 and 14 days. * Indicates the statistical significance with $p < 0.05$.

Table 1

Samples	Lattice parameters (Å)	Average crystallite size (± 1 nm)	Crystallinity of (002) plane (%)
WBS	a & b=9.24±0.22 c=6.87±0.27 V=520.72	80	47
EBS	a & b=9.34±0.14 c=6.99±0.35 V=529.47	60	24

Table 2

Compressive strain (%)	Compressive strength (MPa)		Compressive Modulus (MPa)	
	WBS	EBS	WBS	EBS
10	0.70±0.40	0.72±0.31	8.57±0.92	7.9±1.00
25	3.75±0.51	2.74±0.35	24.80±2.51	18.74±3.95
50	12.23±0.39	9.45±0.59	60.88±1.54	48.95±4.98

Table 3

Sample code	Diameter of zone (cm) (mean± SD)						
	Pseudomonas			Bacillus			
	9h	12h	24h	6h	9h	12h	24h
EBS-GS	4.0±0.1	4.2±0.1	4.2±0.1	2.8±0.2	3.3±0.2	3.9±0.1	4.0±0.1
WBS-GS	1.6±0.2	2.8±0.3	3.5±0.2	2.3±0.1	2.4±0.2	3.0±0.2	3.5±0.1
EBS-AMX	2.5±0.2	3.1±0.1	3.2±0.1	1.0±0.1	1.1±0.1	1.2±0.1	1.2±0.1
WBS-AMX	3.1±0.1	3.5±0.1	3.6±0.1	1.2±0.1	1.3±0.1	1.5±0.1	1.5±0.1

Figure 1

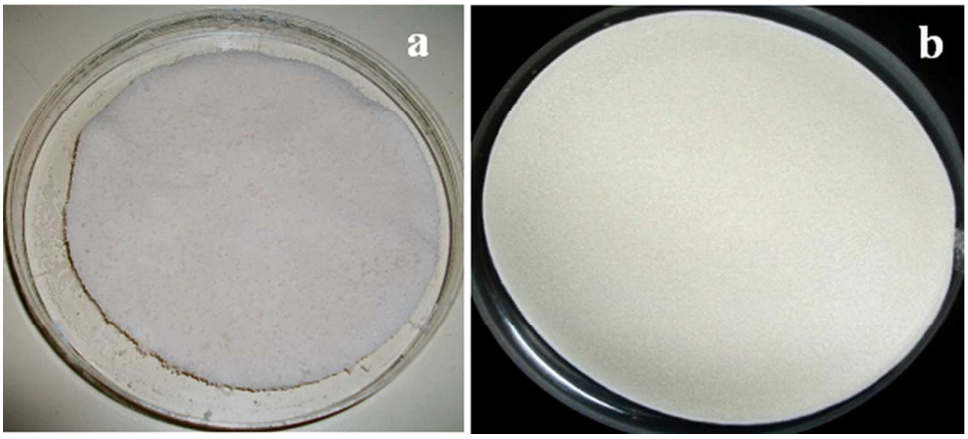

Figure 2 (a and b)

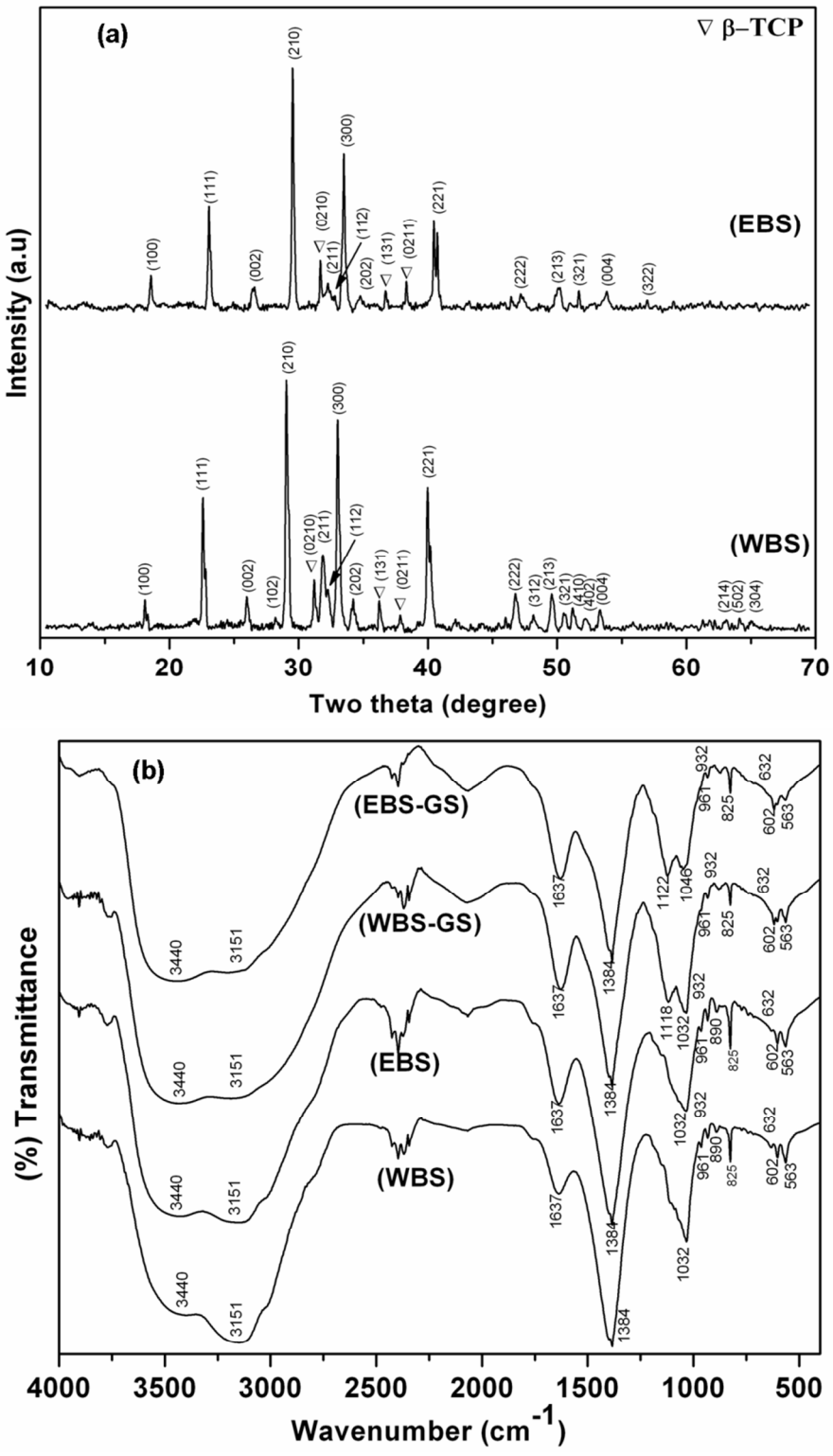

Figure 2 (c)

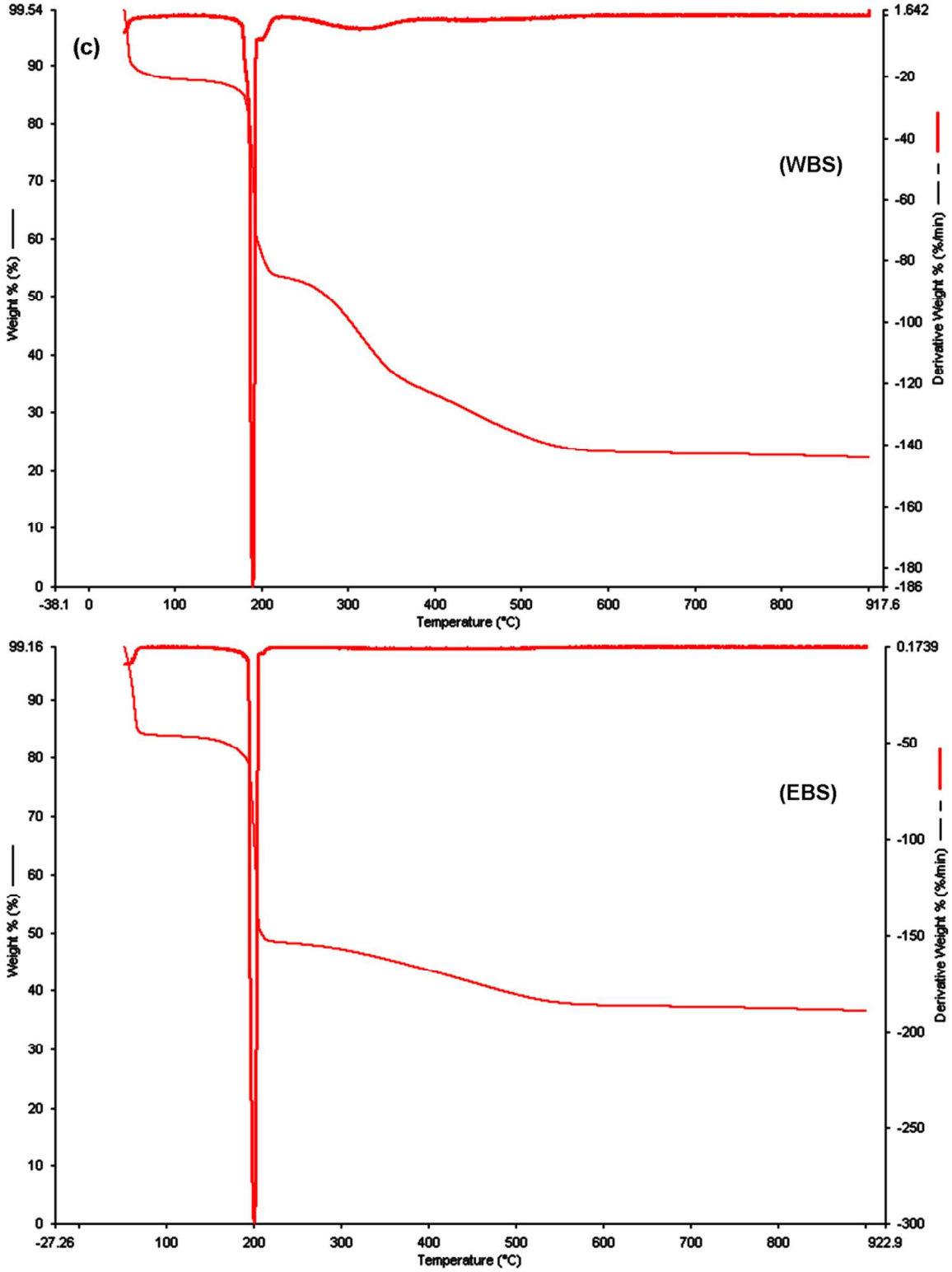

Figure 3

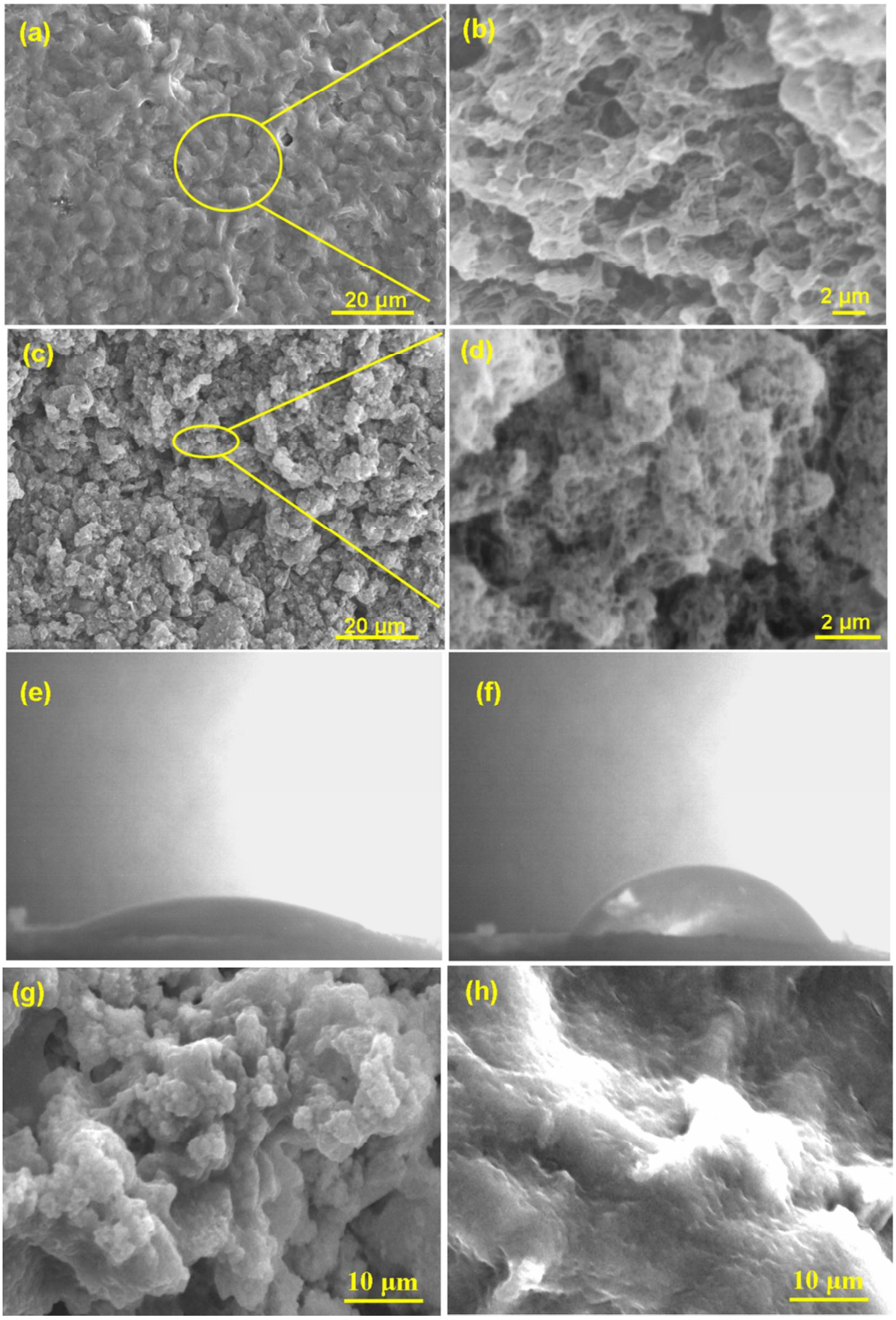

Figure 4

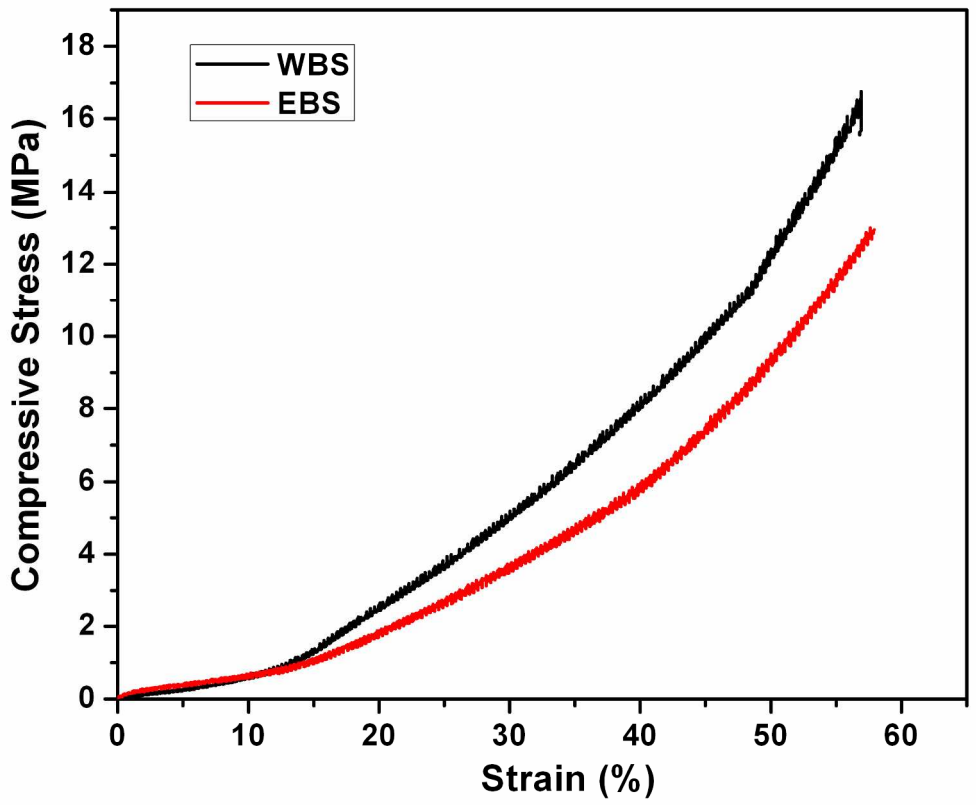

Figure 5

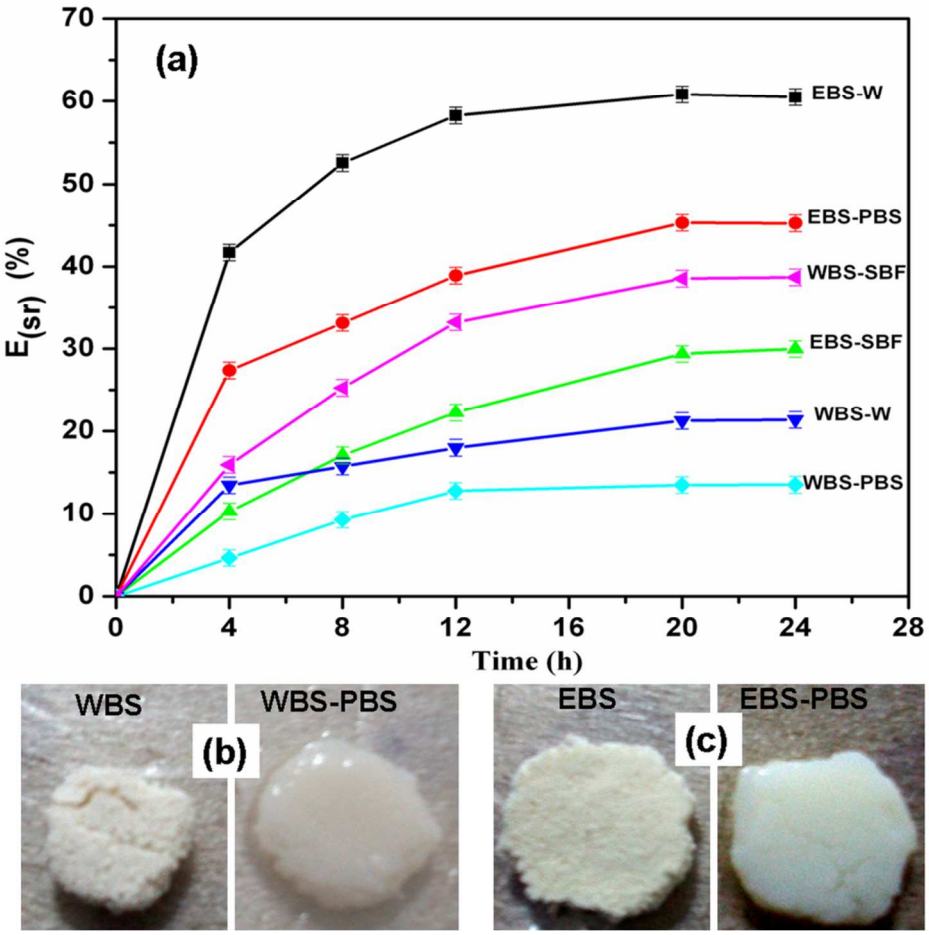

Figure 6

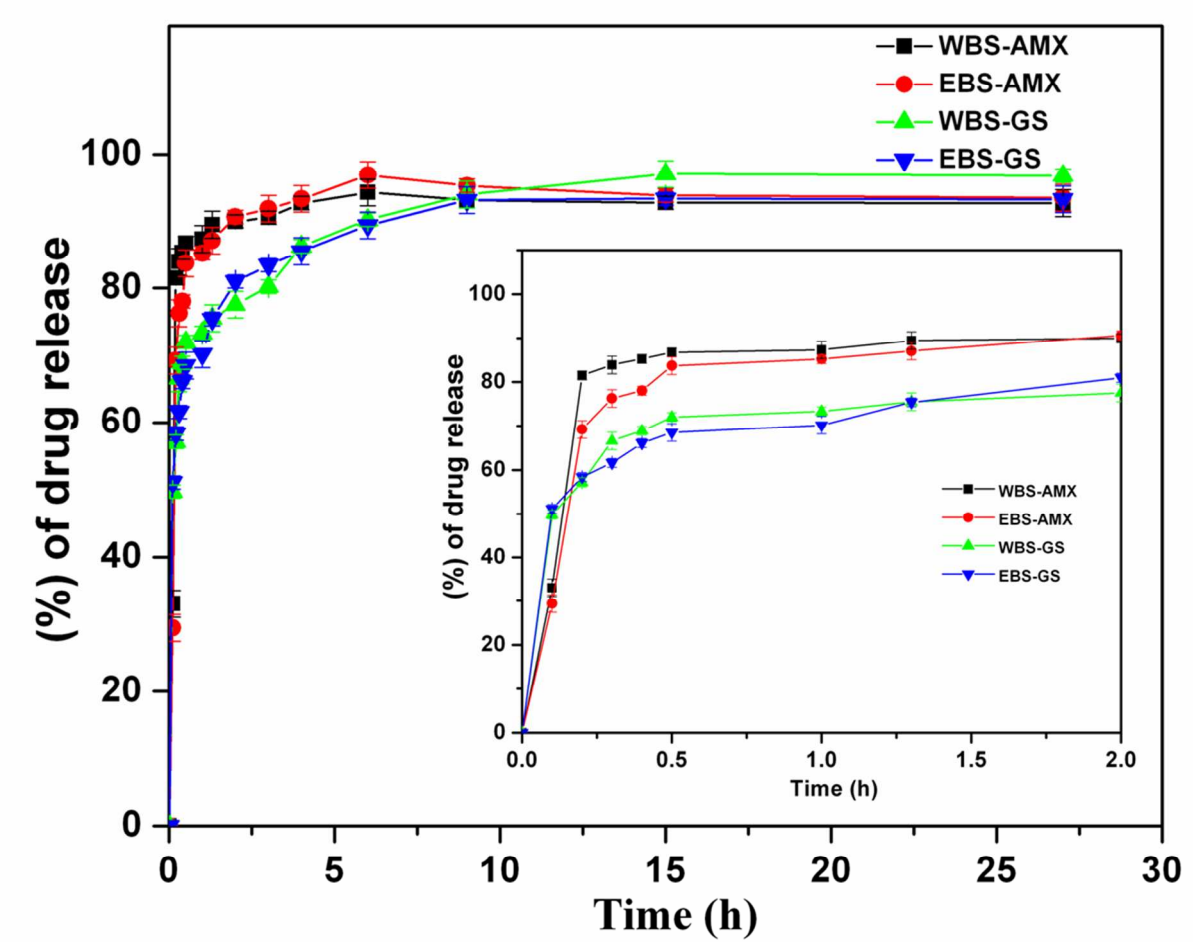

Figure 7

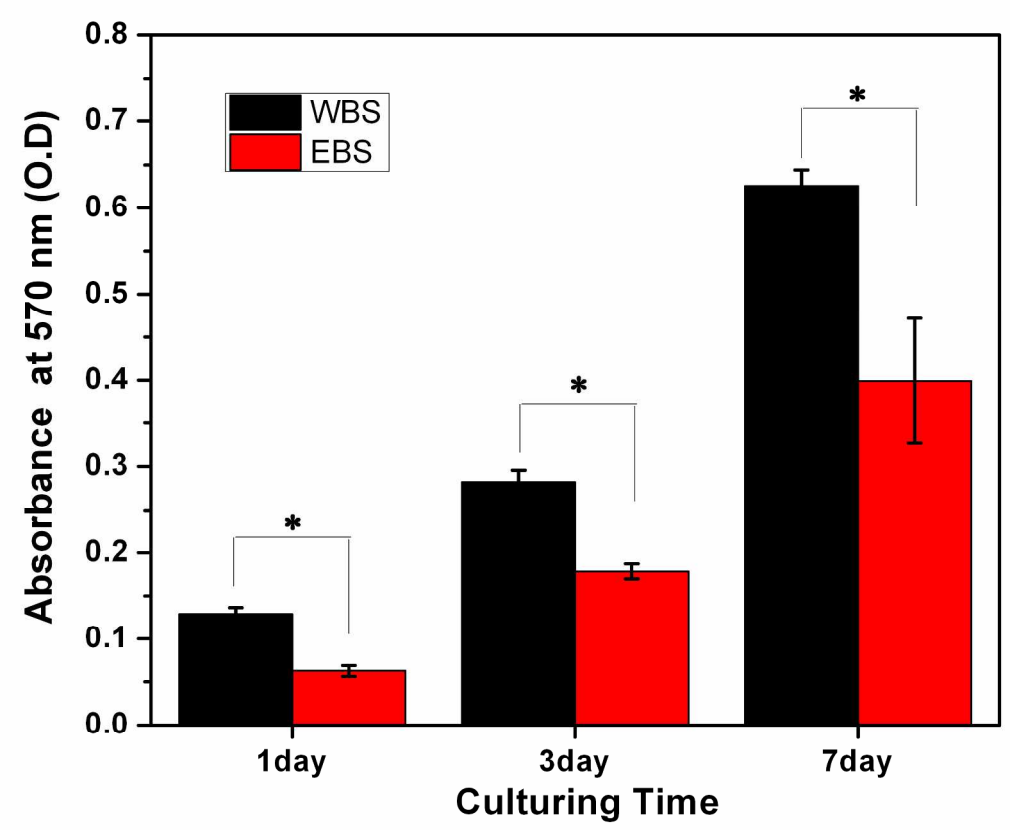

Figure 8

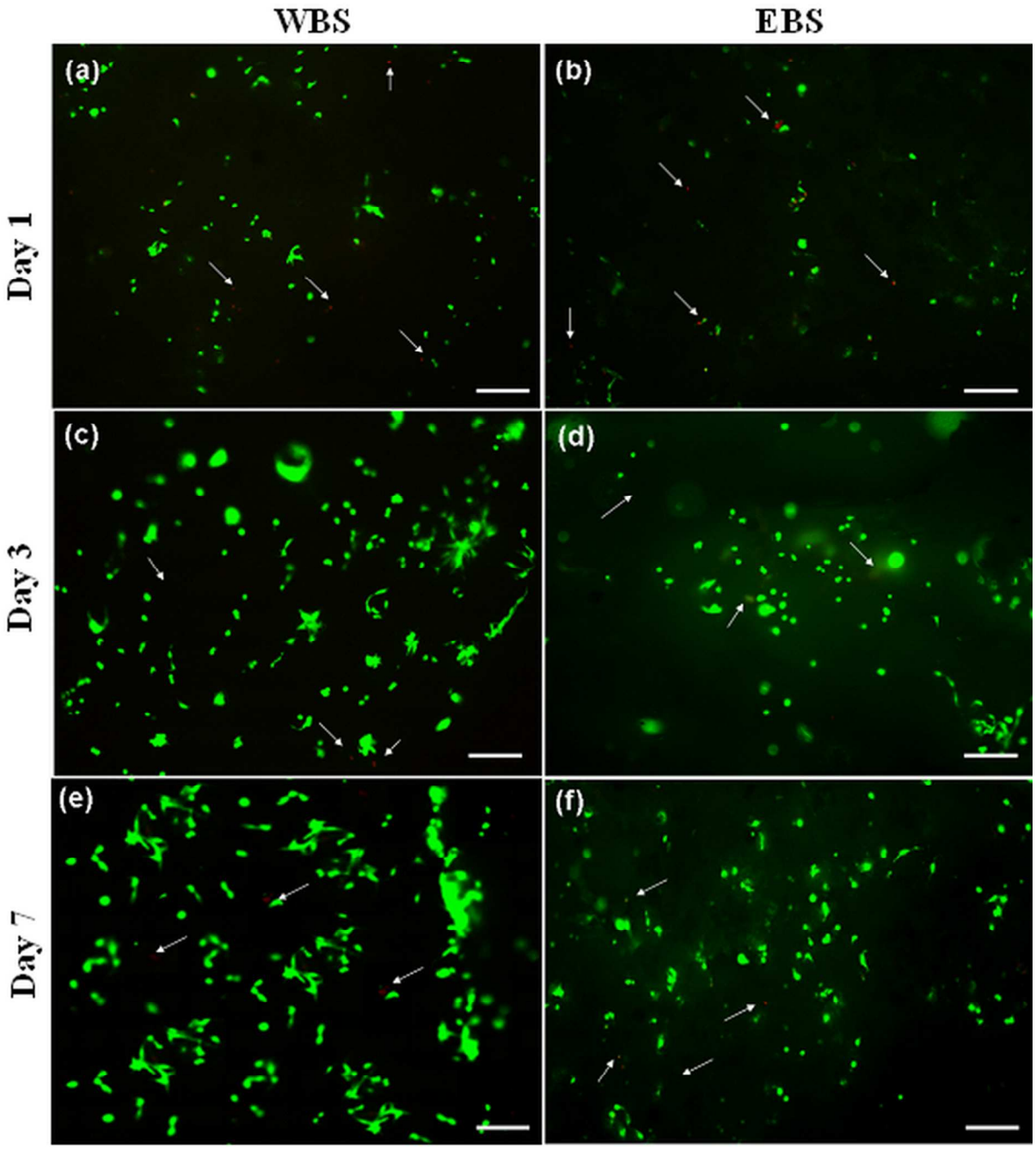

Figure 9

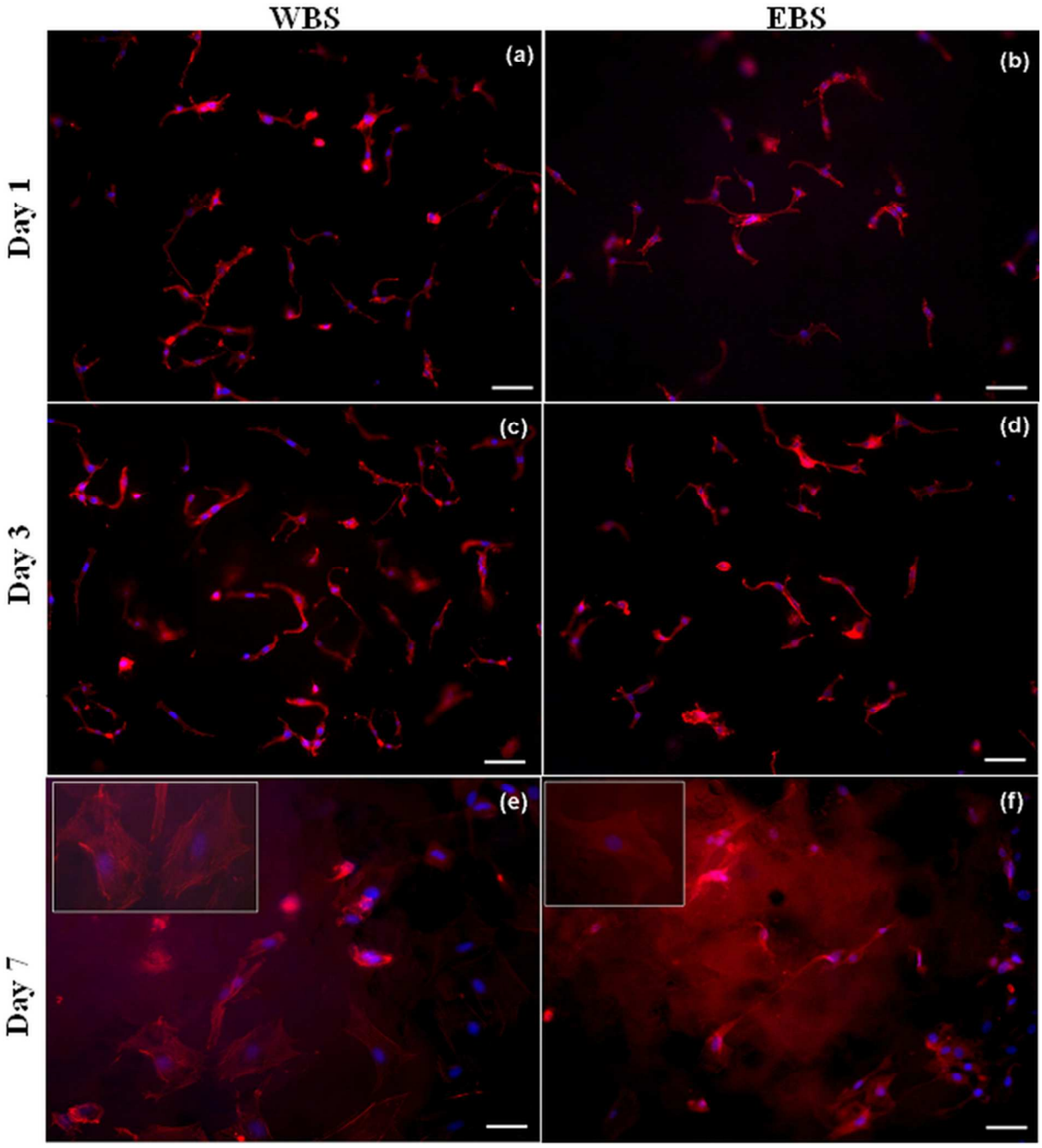

Figure 10

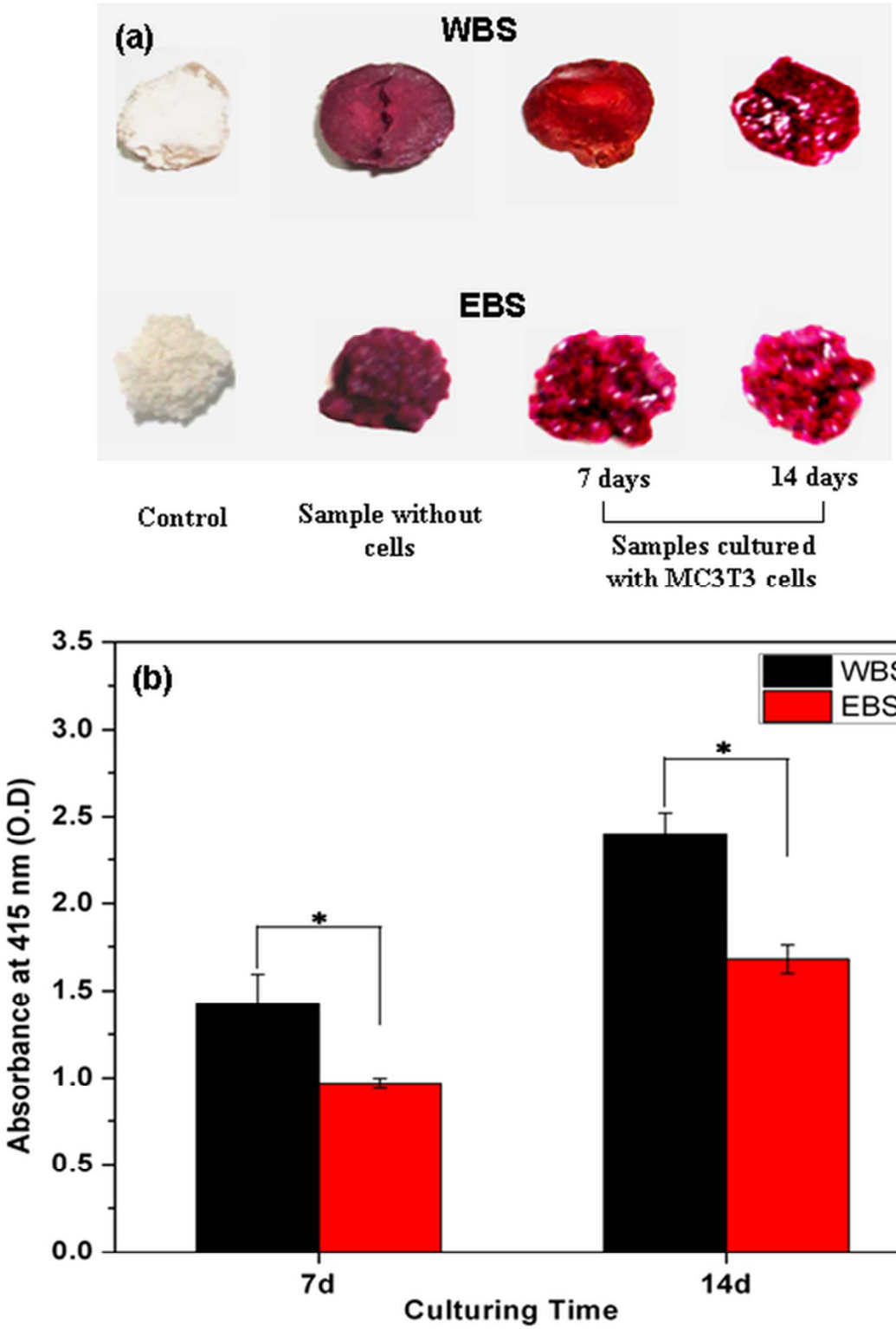

Table of content (TOC) Figure